Optik 125 (2014) 1320–1324

Contents lists available at ScienceDirect

Optik

journal homepage: www.elsevier.de/ijleo

Analysis of the fringes visibility generated by a lateral cyclic shear interferometer in the retrieval of the three-dimensional surface information of an object

Analia Sicardi-Segade[a,*], Amalia Martínez-García[a], Noel-Ivan Toto-Arellano[b], J.A. Rayas[a]

[a] Centro de Investigaciones en Óptica, A. C., León, Guanajuato, Mexico
[b] Universidad Tecnológica de Tulancingo, Hidalgo, Mexico

ARTICLE INFO

Article history:
Received 5 April 2013
Accepted 5 August 2013

Keywords:
Optical metrology
Projected fringes
Fringes visibility
Interferometry
Lateral cyclic shear interferometer

ABSTRACT

We report the evaluation of the topography of an object with projected fringes generated with a lateral cyclic shear interferometer (CSI) and we then compare the topography recovery obtained with the proposed method with the one obtained from a coordinate measuring machine (CMM). We also study how the fringes visibility along the *z* axis affects the retrieval. Finally, we discuss the advantages and drawbacks of this profilometry system.

© 2013 Elsevier GmbH. All rights reserved.

1. Introduction

During the last years, the use of the fringe projection technique for generating three-dimensional (3D) surface information has become one of the most active research areas in optical metrology [1]. The retrieval of the three-dimensional shape of an object is an issue of great interest for a wide range of applications such as heritage protection, industrial, technical and medical applications [2,3].

Coordinates measurement machines (CMMs) are well established and widely accepted in many applications. However, CMMs possess some limitations such as a high cost, a low measurement speed and the sparseness of the measurement points [3]. Common optical methods for surface profiling include the use of moiré and holographic interferometry, fringe projection and others [4]. Among them, the fringe projection method is considered the simplest one because optical fringes can be generated and projected easily with a Michelson interferometer [5]. But the use of this type of interferometer requires stringent vibration-free testing conditions, thereby confining its applications to the laboratory environment [4].

In this paper we present a lateral cyclic shear interferometer (CSI) to generate projected fringes. This interferometer has the advantage of generating stable fringes with little vibration isolation.

We also evaluate the influence of the visibility of the fringes and how these affect the recovery of the topography by analyzing the visibility as a function of the distance between the object and the projection system, and as a function of the laser power too, and we compare the retrieval of the test object for some values of the *z* axis, with the retrieval obtained from a CMM. Finally, we calculate the experimental resolution of the optical system as a function of the distance.

2. Experimental set-up

Lateral shearing interferometry is an important field of interferometry and has been used extensively in diverse applications such as the testing of optical components and systems and the study of flow and diffusion phenomena in gases and liquids [6–9]. Basically the method of lateral shearing interferometry consists of displacing the wavefront laterally by a small amount and obtaining the interference pattern between the original and the displaced wavefronts [6]. The beams centers are separated by a distance Δs, called *shear distance* [9]. The shear interferometer produces an interference pattern that is proportional to the slope of the wavefront [10]. Shear interferometers have been used to determine the shape of

* Corresponding author. Tel.: +52 477 4 41 42 00; fax: +52 477 4 41 42 09.
E-mail addresses: analia@cio.mx (A. Sicardi-Segade), amalia@cio.mx (A. Martínez-García), ivantotoarellano@hotmail.com (N.-I. Toto-Arellano), jrayas@cio.mx (J.A. Rayas).

0030-4026/$ – see front matter © 2013 Elsevier GmbH. All rights reserved.
http://dx.doi.org/10.1016/j.ijleo.2013.08.011

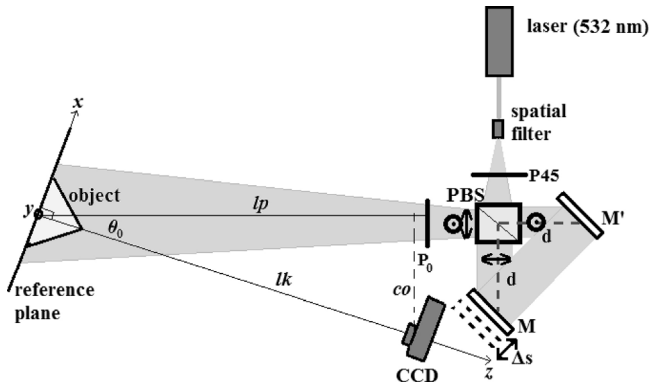

Fig. 1. Fringe projection system using a CSI. (M and M′: mirrors, PBS: polarized 50:50 beam-splitter, P45: linear polarizing filter placed at 45° with respect to the laser polarized light, P_0: linear polarizing filter used to make both beams components interfere, l_p: distance between the array and the reference plane, l_k: distance between the camera CCD and the reference plane and θ_0 is the angle between l_p and l_k.

the objects by contouring, but calculating the spatial derivatives of the surface topography [7,8]. By using this method, the spatial derivatives are obtained and then they are integrated to obtain the shape of the objects. However, in this technique, the noise in the experimental data affects numerical integration.

In Fig. 1, the CSI used as a fringe projection system is showed, where the shear is generated by moving the mirror M by a small distance Δs. A Verdi laser emitting at *532* nm (2 W maximum output power), was expanded and spatially filtered using a 60× microscope objective lens and a 20 μm diameter pinhole. We used divergent illumination and output laser powers of 20, 40, 60 and 80 mW.

The fringe pattern is generated as follows. Light passes through the spatial filter and then through the first linear polarizing filter placed at 45° with respect to the laser's polarized light transmission axis. After that, the light beam passes through the polarized beam-splitter (PBS), where it is divided into two beams. The beam-splitter is designed to transmit one of the beams with a horizontal polarization, while the other one is reflected with a vertical polarization. Both beams are reflected in the two mirrors M and M′, that are placed initially at a distance d from the beam-splitter. The vertical polarized beam arrives to mirror M′ and is reflected to mirror M, where it is reflected back to the PBS. The horizontal polarized beam arrives to mirror M where it is reflected to mirror M′ before arriving to the PBS. When both beams get outside the polarized beam-splitter, one beam polarization is perpendicular to the other one and a polarizing linear filter P_0 is needed in order to make that both beams components interfere [11,12]. The fringe pattern can then be seen in a reference plane, and the fringes pitch can be adjusted by moving the mirror M.

The use of the polarizing filters and the PBS is to obtain the best visibility. The fringes pattern can also be obtained by using a non-polarizing 50:50 beam-splitter and without the polarizing filters, but in that case the visibility of the fringe-pattern would be smaller because the transmission and reflection beams are not exactly 50:50 in practice, that is, there is a little difference between the two beams. By using the polarizing filter and the PBS we can obtain the best contrast rotating the polarizing filter P_0 to find the best visibility.

In the case of parallel illumination and parallel observation, the equation to retrieve the three-dimensional shape is [13]

$$z = \frac{\Delta\phi * p}{2 * \pi * \tan\theta_0}, \tag{1}$$

where p is the fringes pitch and $\Delta\phi$ is the phase difference between the test object and the reference plane.

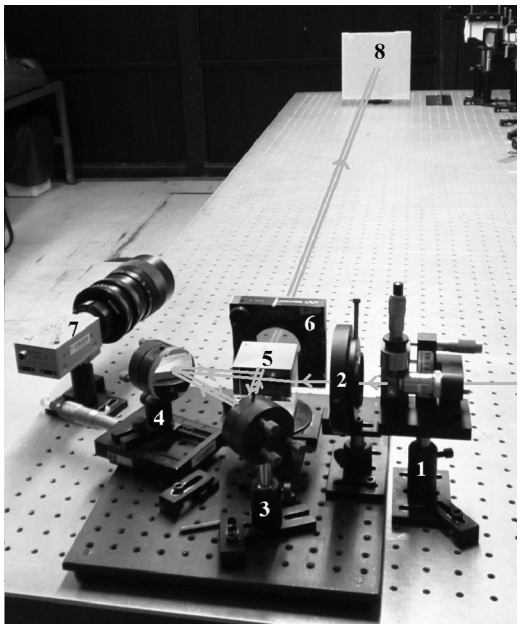

Fig. 2. Experimental array. 1. Spatial filter, 2. polarizer placed at 45° with respect to the laser's polarized light transmission axis, 3. mirror, 4. mobile mirror, 5. PBS: polarized beam-splitter, 6. linear polarizing filter used to make both beams components interfere, 7. CCD, 8. reference plane. The arrows show the beam path.

With the use of non-collimated illumination the topography can be obtained by the following two equations [3,13]

$$z = \Delta\phi * S, \tag{2}$$

where S [mm/rad] is the sensitivity of the system and it depends on the set-up geometry [3,13], and

$$S = \frac{p_{xo}}{2 * \pi} * \cos\theta_0 * \left[\sin\theta_0 + \frac{(l_k - l_p * \cos\theta_0) * x}{l_p * l_k}\right]^{-1} * \left[1 + \frac{x * \sin\theta_0}{l_p}\right]^2, \tag{3}$$

where p_{xo} is the pitch of the fringe at $x = 0$, θ_0 is the angle between the projection and the observation directions, l_p is the distance between the polarizer P_0 of the CSI and the reference plane for $x = 0$, and l_k is the distance between the CCD and the reference plane at $x = 0$ [3].

3. Results and discussion

In this section we present some experimental results of the fringe projection profilometry system used to retrieve the three-dimensional shape of an object. The test object is a pyramid with a base of 89 mm × 89 mm and a height of 48 mm. Fig. 2 shows the experimental optical system used to project fringes over the test object, Fig. 3 shows the pyramid with the projected fringes, Fig. 4a shows the topography obtained by measuring some points with a CMM and Fig. 4b shows the topography obtained by using the projected fringes technique. To retrieve the object with the CMM method, 41 surface points were measured. After that, interpolation and extrapolation were necessary to complete the surface and to recover the topography of the pyramid.

The Fourier-transform technique was used to recover the wrapped phase of the projected fringe pattern [14]. To unwrap the phase of the object, a noise robust algorithm was programmed [15].

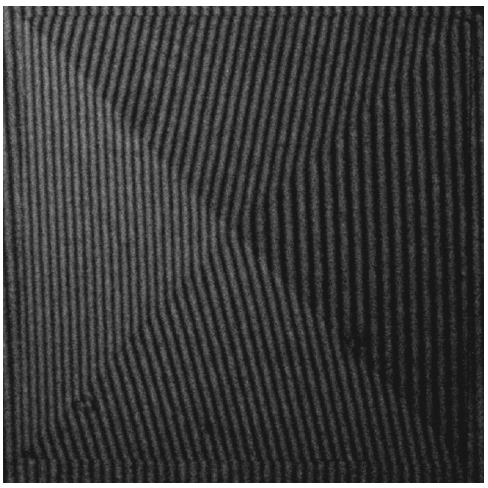

Fig. 3. Fringes projected on a white pyramid.

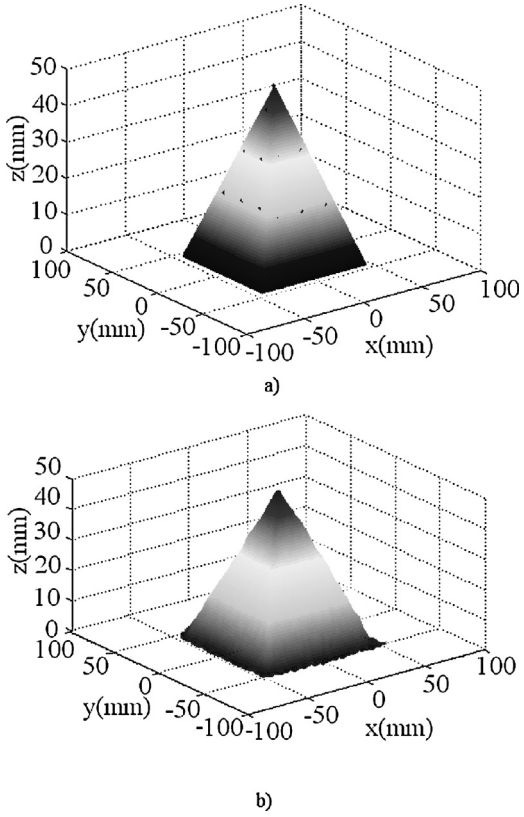

Fig. 4. Topography of the pyramid obtained by (a) measurements from the CMM and (b) our fringe-projection technique.

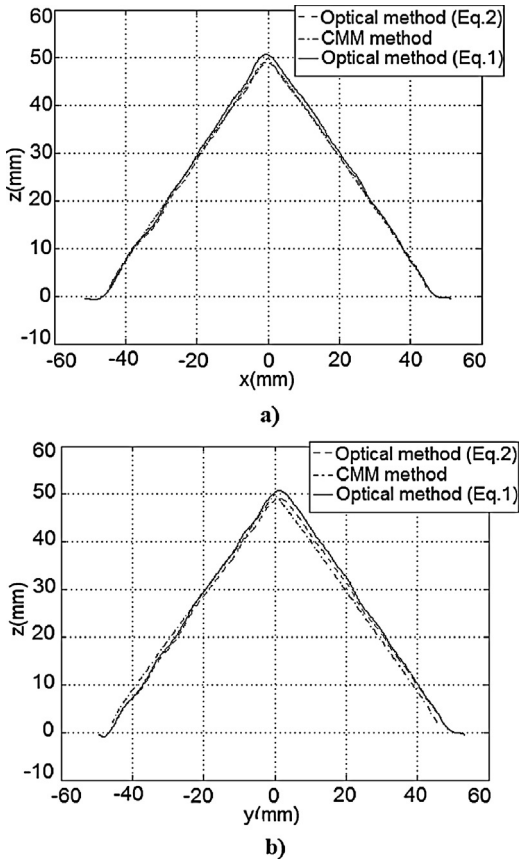

Fig. 5. Measurements obtained from the CMM (dashed-point line) and the optical method by using Eq. (1) considering collimated illumination (continuous line) and Eq. (2), non-collimated illumination (dashed line), in (a) $y = 0$ and (b) $x = 0$.

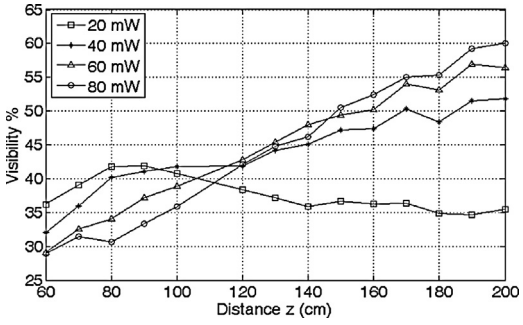

Fig. 6. Visibility as a function of distance for different laser powers.

The experimental results obtained with the projected fringes technique by using Eq. (2) in the case of non-collimated illumination, show a maximum error of 4.5% in the topography measurement, taking as a reference the measurement obtained with the CMM. In this case, the distance between the reference plane and CCD was $l_k = 160$ cm and the distance between the projection head and the reference plane was $l_p = 158.9$ cm. The laser output power was 60 mW.

Fig. 5 shows topography profiles by using Eqs. (1) and (2), which are compared with profile obtained from the CMM in (a) $y = 0$ and (b) $x = 0$. It can be observed that the topography evaluated by using Eq. (2), which takes into account the divergent illumination, is close to the topography obtained by the CMM.

4. Analysis of the projected fringes visibility generated by a CSI

The fringe pattern is recorded by a CCD at different positions along the optical axis. The distance between the reference plane center and the CCD is from 60 cm to 200 cm. The fringe pattern is recorded each 10 cm. The output power of the laser used was 20, 40, 60 and 80 mW, at every position of the CCD. Fig. 6 shows the fringes visibility as a function of the distance between the reference plane center and the CCD for the different powers employed.

As can be seen from Fig. 6, the visibility obtained at the CCD positions between 60 cm and 90 cm is higher for the lowest power used, that is, 20 mW. This is due to the saturation of the CCD for

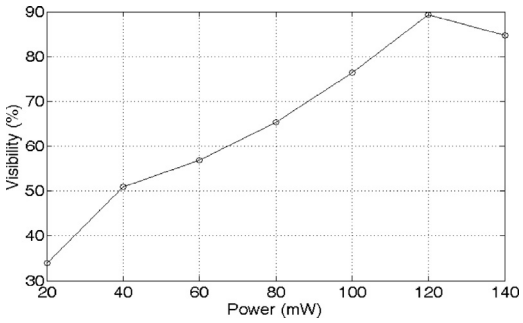

Fig. 7. Visibility versus laser's power at $z = 200$ cm.

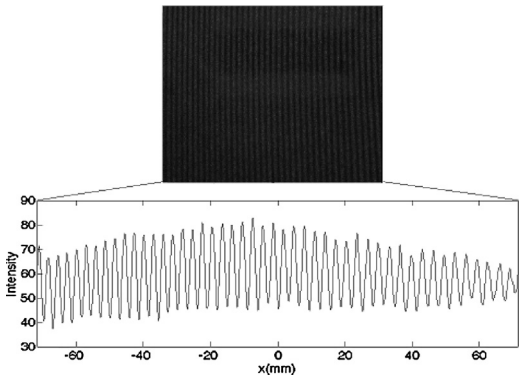

Fig. 8. Fringe pattern and its intensity profile.

powers larger than 20 mW. However, 20 mW is not enough power for distances greater than 90 cm and the fringes visibility decrease. For distances longer than 90 cm higher powers are needed in order to increase the fringes visibility. In the CCD position corresponding to 200 cm, the best visibility is obtained for a power of 80 mW (up to 60%). Next, we fixed the distance at 200 cm and changed the laser power in order to find the power that increases the fringes visibility. Fig. 7 shows that a visibility of 89% is reached for a power of 120 mW. For higher values, the visibility decreases due to the saturation of the CCD. The visibility (or contrast) was calculated by using the following equation [16]

$$V = \frac{I_{\max} - I_{\min}}{I_{\max} + I_{\min}}. \tag{4}$$

The visibility was calculated by considering the average intensity of each column of the fringe pattern and then calculating the maximum and the minimum intensity of the resulting array. Fig. 8 shows a fringe pattern and its intensity profile used to determine the visibility.

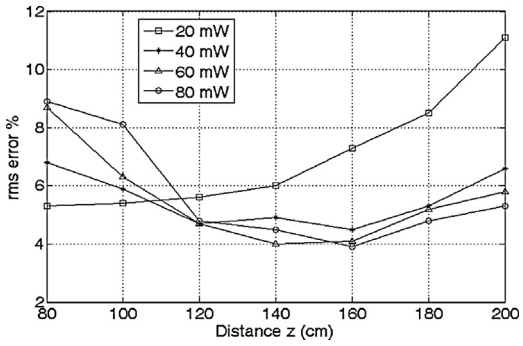

Fig. 9. Curves of topography error versus distance for different powers.

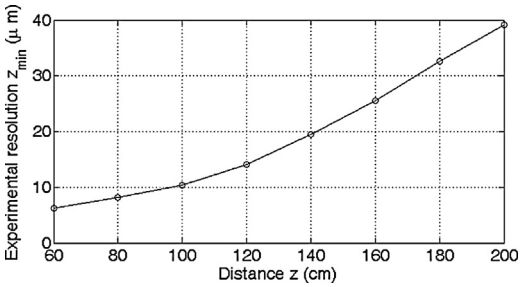

Fig. 10. Experimental resolution of the system versus distance.

Fig. 9 shows the root-mean-square error (rms) associated to the topography measurement versus CCD position and for different laser powers. It is observed that the fringes visibility affects the measurement of the topography. We found a maximum error in the topography measurement of 9% for a power of 80 mW with the CCD placed at 80 cm to the reference plane. In this same CCD position, an error of 5.4% is obtained for a power of 20 mW. At 200 cm, the error increases to 11% for a power of 20 mW while the error decreases to 5.3% when the power used is 80 mW. The error was calculated based on the measurements obtained from the CMM.

Finally, we calculated the experimental resolution of the optical system, i.e. the minimum z that can be measured. To calculate the minimum z, Eq. (1) was used considering that the fringe moves one period when the object is placed instead of the reference plane. Assuming that, the relation $\Delta\phi/(2\times\pi) = N = order\ of\ the\ fringe = 1$ holds. As a consequence, Eq. (1) can be written as [17]

$$\Delta z = \frac{p}{\tan\theta_0}. \tag{5}$$

Now, to calculate the $z_{\min}$, we consider the fringe moving only one pixel in one period, that is

$$z_{\min} = \frac{\Delta z}{number\_of\_pixel\_per\_period} = \frac{\frac{p}{\tan\theta_0}}{number\_of\_pixel\_per\_period}. \tag{6}$$

Fig. 10 shows the experimental resolution obtained as a function of the distance. It can be seen that the resolution improves when the distance between the optical system and the reference plane is decreased.

5. Conclusions

In this work we proposed a linear cyclic shear interferometer to generate projected fringes. Being a cyclic path this interferometer is quite stable, therefore one of the advantages of this method is its capability to generate stable fringes in poor vibration isolation conditions.

The fringe-pattern projected by an interferometric system has the advantage of being absolutely sinusoidal, unlike the one generated with a multimedia projector. Moreover, with a fringe projection interferometer, synchronization with a CCD camera is not necessary.

By using this method, the pitch of the fringes can be varied by changing Δs, which means that both large and small objects can be measured.

One of the disadvantages of this optical system is that the size of the object to be measured is limited by the size of the beam-splitter, which imposes a limit to the expansion of he beam to cover a large object placed at a short distance.

In this work, we also presented an analysis of how the visibility of projected fringes affects the evaluation of the topography of an object by using fringes generated by interferometry.

Acknowledgements

This research has been supported by the Consejo Nacional de Ciencia y Tecnología (CONACYT) through grant 180449. Analia Sicardi-Segade thanks CONACYT for her scholarship.

References

[1] S.S. Gorthi, P. Rastogi, Fringe projection techniques: whither we are? Opt. Lasers Eng. 48 (2) (2010) 133–140.
[2] F. Chen, G.M. Brown, M. Song, Overview of three-dimensional shape measurement using optical methods, Opt. Eng. 39 (1) (2000) 10–22.
[3] A. Martínez, J.A. Rayas, H.J. Puga, K. Genovese, Iterative estimation of the topography measurement by fringe-projection method with divergent illumination by considering the pitch variation along the *x* and *z* directions, Opt. Lasers Eng. 48 (2010) 877–881.
[4] M.I.R.B. Zainal A., G.L.M. Jie, M. Wee, T. Lai, Y. Fu, H.M. Shang, A simple laboratory set-up for the fringe-projection method, Proc. SPIE 4588 (2002).
[5] G.N. de Oliveira, M.E. de Oliveira, P.A.M. dos Santos, Dynamic moiré patterns and Michelson fringe patterns for profilometry: a results comparative analysis, Proc. SPIE 8011 (2011), 80110J-1.
[6] D. Malacara, Lateral shearing interferometers, Chap. 4 in Optical Shop Testing, second ed., Wiley, New York, 1992.
[7] T. Santhanakrishnan, P.K. Palanisamy, R.S. Sirohi, Optical configuration in speckle shear interferometry for slope change contouring with a twofold increase in sensitivity, Appl. Opt. 37 (16) (1998).
[8] P.K. Rastogi, An electronic pattern speckle shearing interferometer for the measurement of surface slope variation of three-dimensional objects, Opt. Lasers Eng. 26 (1997) 93–100.
[9] R.K. Tyson, Wavefront sensing, series in optics and optoelectronics, Chap. 5 in Principles of Adaptive Optics, third ed., CRC Press Taylor & Francis Group, 2011.
[10] N.I. Toto-Arellano, A. Martínez-García, G. Rodríguez-Zurita, J.A. Rayas-Álvarez, A. Montes-Perez, Slope measurement of a phase object using a polarizing phase-shifting high-frequency Ronchi grating interferometer, Appl. Opt. 49 (2010) 6402–6408.
[11] D.I. Serrano-García, N.I. Toto-Arellano, A. Martínez García, J.A. Rayas Álvarez, A. Téllez-Quiñonez, G. Rodríguez-Zurita, Simultaneous phase-shifting cyclic interferometer for generation of lateral and radial shear, Revista Mexicana de Física 57 (3) (2011) 255–258.
[12] N.I. Toto-Arellano, D.I. Serrano-García, A. Martínez García, G. Rodríguez Zurita, A. Montes-Pérez, 4D profile of phase objects through the use of a simultaneous phase shifting quasi-common path interferometer, J. Opt. 13 (2011), 115502 (8pp).
[13] K.J. Gasvik, Moire methods. Triangulation, Chap. 7 in Optical Metrology, third ed., John Wiley & Sons, Ltd., 2002.
[14] M. Takeda, H. Ina, S. Kobayashi, Fourier-transform method of fringe-pattern analysis for computer-based topography and interferometry, J. Opt. Soc. Am. 72 (1982) 156–160.
[15] J.C. Estrada, M. Servin, J.A. Quiroga, Noise robust linear dynamic system for phase unwrapping and smoothing, Opt. Express 19 (6) (2011) 5126–5133.
[16] T. Kreis, Optical foundations of holography, Chap. 2 in Holographic Interferometry: Principles and Methods, Akademie Verlag Series Optical Metrology, vol. 1, Akademie Verlag, Bremen, 1996, pp. 21–22.
[17] K.J. Gasvik, Moire techniques by means of digital image processing, Appl. Opt. 22 (23) (1983).